Mesoscopic modelling of columnar solidification

Miha Založnik, Alexandre Viardin, Youssef Souhar, Hervé Combeau, Markus Apel

Mesoscopic modelling of columnar solidification

2016 IOP Conf. Ser.: Mater. Sci. Eng. 117 012013

(http://iopscience.iop.org/1757-899X/117/1/012013)

IOP Conf. Series: Materials Science and Engineering **117** (2016) 012013 doi:10.1088/1757-899X/117/1/012013

Mesoscopic modelling of columnar solidification

M Založnik[1], A Viardin[2], Y Souhar[1], H Combeau[1], M Apel[2]

[1] Institut Jean Lamour, CNRS – Université de Lorraine, F-54011 Nancy CEDEX, France
[2] Access e.V., Intzestr. 5, D-52072 Aachen, Germany

E-mail: miha.zaloznik@univ-lorraine.fr

Abstract. We used two complementary modeling approaches for the simulation of columnar growth in directional solidification of organic alloys: a phase-field model and a mesoscopic envelope model of dendritic growth. While the phase-field method captures the details of the dendritic structure and of the growth dynamics, the mesoscopic model approximates the complex dendritic morphology by its envelope. The envelope growth is deduced from the velocities of the dendrite tips, calculated by an analytical LGK-type tip model that is matched to the heat and concentration fields in the stagnant film around the envelope. The computational cost of the mesoscopic model is several orders of magnitude lower and can bridge the gap between phase-field and macroscopic models. We demonstrate the applicability of the mesoscopic model to columnar growth and discuss its possibilities and limitations by comparisons with phase-field simulations for the same conditions.

1. Introduction

The patterns and the dynamics of the nonlinear growth of solidification microstructures are studied with much success using phase-field methods. Phase-field models have been developed into efficient tools giving quantitative results. However, as in any model, its application is subject to certain limitations, mainly due to the necessary computing power. The mesoscopic solidification model of Steinbach, Beckermann et al. [1, 2] offers a complementary tool for the study of dendritic solidification. It can be applied at larger scales, in three dimensions and can include fluid flow at acceptable computing cost. The mesoscopic model is thus more convenient for the study of the dynamics of ensembles with a higher number of dendrites or phenomena that contain larger length and time scales, such as the CET. Computational efficiency is achieved at the price of several simplifications. The details of the dendritic structure are not resolved. Instead, the complex morphology is approximated by its envelope and by a field of phase fractions in the interior of the envelope. Also, the selection of the dendrite-tip operating state is not predicted by the model. The growth of the envelope is deduced from the velocities of the dendrite tips, calculated by an analytical LGK-type tip model that is matched to the concentration fields in the stagnant film around the envelope. Information from the microscopic scale is required to determine the tip selection parameter σ^* and the thickness of the stagnant film.

The mesoscopic model was applied to equiaxed dendritic growth in pure metals [1, 2] and in alloys [3, 4]. It was demonstrated that it can accurately predict envelope shapes of equiaxed dendrites as well as the dynamics of their interactions. The only application of the mesoscopic model to columnar growth was developed by Delaleau et al. [3], who compared the model to in-situ X-ray experiments of solidification of thin samples. To reproduce the experimental conditions, the same disposition of grain nuclei as observed in the experiment was introduced

in their simulations. The dynamics of primary spacing selection in columnar growth has been recently successfully modeled by the meso-scale DNN model [5]. Another meso-scale approach was attempted by the so-called tuned cellular-automaton model [6], alas requiring strong unphysical adjustments of the parameters in order to obtain primary spacings of a realistic order of magnitude.

The question whether the mesoscopic model can address the mechanism of spacing selection in columnar growth remained open. Spacing selection is determined by both, the operating state of a single dendrite tip, i.e. its tip radius, and the solutal interaction between neigboring dendrites [7]. While the mesoscopic model should give an accurate representation of solutal interactions, the tip selection, a consequence of the anisotropy of the interface energy, is, clearly, strongly simplified. It is included implicitly (at a larger scale) by its consequences: the selection parameter and the tip growth directions.

In this paper we demonstrate the applicability of the mesoscopic model to spacing selection in columnar growth. As a reference we use phase-field simulations in 2D. We study directional solidification of a transparent organic alloy,. We compare simulations with the two models for the same conditions and we show that the primary arm spacing can be correctly reproduced by the mesoscopic model.

2. The mesoscopic envelope-field model

The core idea of the mesoscopic envelope model [1, 2] is the description of a dendritic grain by its envelope – a virtual smooth surface that links the tips of the actively growing dendrite branches. The velocity of the envelope growth can thus be calculated from the velocities of the dendrite tips. The growth of the dendrite tips is controlled by the solute flux that they reject into their surroundings and is therefore determined by the local conditions in the proximity of the envelope. The branched dendritic structure inside the envelope is only implied and its details are not resolved; the interior of the envelope is rather described in a volume-averaged sense by a phase-fraction field and other volume-averaged quantities. The phase change that determines the evolution of the structure inside the growing envelope is controlled by the solute exchange with the surroundings of the grain.

The model used to describe the kinetics of the dendrite tips is based on the analytical solution of the growth of a single isothermal parabolic tip in an infinite undercooled melt. The classical Ivantsov solution of this problem, recast by Cantor & Vogel [8], gives the supersaturation Ω_δ of the melt at a finite distance δ from the tip with a curvature radius R_{tip} as a function of the tip Péclet number, $\mathrm{Pe}_C = R_{\mathrm{tip}} V_{\mathrm{tip}}/(2D_{\mathrm{l}})$. To determine unique values for the tip velocity and radius, an additional tip selection criterion is required. In the case of a solutally controlled tip (limit of high Lewis numbers) the selection criterion is of the type $R_{\mathrm{tip}}^2 V_{\mathrm{tip}} = \mathrm{const}$. The tip velocity and radius are then given by the system of the Cantor-Vogel function (here for a 2-dimensional tip) and the tip selection criterion, as a function of the local supersaturation Ω_δ:

$$\Omega_\delta = \sqrt{\pi \mathrm{Pe}_C}\, \exp\left(\mathrm{Pe}_C\right) \left[\mathrm{erfc}\left(\sqrt{\mathrm{Pe}_C}\right) - \mathrm{erfc}\left(\sqrt{\mathrm{Pe}_C \left[1 + \tfrac{2\delta}{R_{\mathrm{tip}}}\right]}\right)\right] \; ; \quad R_{\mathrm{tip}}^2 V_{\mathrm{tip}} = \frac{d_0 D_{\mathrm{l}}}{\sigma^*}. \quad (1)$$

$d_0 = \Gamma/(m_{\mathrm{L}} C_{\mathrm{l}}^* (k_{\mathrm{p}} - 1))$ is the solutal capillary length, σ^* is the selection parameter, Γ is the Gibbs-Thomson coefficient, m_{L} is the liquidus slope, k_{p} is the binary equilibrium partition coefficient, and C_{l}^* is the concentration in the liquid at the tip interface (i.e. the equilibrium liquid concentration at the given temperature). Equations (1) together give the local tip velocity at any point on the grain envelope. The matching distance δ is a model parameter that is best chosen at the order of the diffusion length $\delta \sim D_{\mathrm{l}}/V_{\mathrm{tip}}$ [4]. In the mesoscopic model the tip growth directions are prescribed, since the key physics for selection of the preferential growth directions is not included. Knowing the local tip velocity and direction, the envelope velocity is

calculated: $\vec{v}_n = V_{\mathrm{tip}}\vec{n}\cos\theta$, where θ is the angle between the normal to the envelope and the closest of the tip growth directions (i.e. the one forming the smallest angle with the normal).

To track the front that represents the envelope we use the sharp interface tracking method by Sun & Beckermann [9]. This method represents the front by a contour of a continuous indicator function. The function is propagated by a phase-field like propagation equation. The transport at the mesoscopic scale is described by volume-averaged equations, valid in the whole domain. They are equivalent to the classical volume-averaged macroscopic models [10]. The phase change is described at a microscopic scale, where Scheil assumptions are applied. The diffusion of solute in the solid phase is neglected at the mesoscopic scale. This leads to the following conservation equations for solute mass in the liquid and the solid phase:

$$g_{\mathrm{l}}\frac{\partial C_{\mathrm{l}}}{\partial t} = D_{\mathrm{l}}\nabla\cdot(g_{\mathrm{l}}\nabla C_{\mathrm{l}}) + C_{\mathrm{l}}(k_{\mathrm{p}}-1)\frac{\partial g_{\mathrm{l}}}{\partial t}\,; \qquad \frac{\partial(g_{\mathrm{s}}C_{\mathrm{s}})}{\partial t} = -k_{\mathrm{p}}C_{\mathrm{l}}\frac{\partial g_{\mathrm{l}}}{\partial t}\,. \tag{2}$$

g_{l} and g_{s} are the liquid and solid phase fraction respectively and D_{l} is the diffusion coefficient in the liquid. This equation is valid inside and outside the envelope. Inside and on the envelope the liquid is assumed to be in thermodynamic equilibrium, such that $C_{\mathrm{l}} = (T - T_{\mathrm{f}})/m_{\mathrm{L}}$, where T is the imposed temperature field. Eq. (2) thus gives the liquid fraction inside the envelope. Outside the envelope $g_{\mathrm{l}} = 1$ and eq. (2) is reduced to the diffusion equation.

3. The phase-field model

In the present work, the multi-phase-field formulation proposed by Steinbach et al. [11, 12] is employed to describe the morphological evolution during the solid-liquid phase transformation. The phase-field method relies on a phase-field parameter which varies continuously from liquid "l" (ϕ=0) to solid "s" (ϕ=1) along the interface of width η. The evolution of the phase-field parameter in time is given by:

$$\dot{\phi}_s = M^a_{sl}(\vec{n})\left[\sigma^a_{sl}(\vec{n})K_{sl} + w\Delta G_{sl}\right] \tag{3}$$

$$K_{sl} = \phi_s\nabla^2\phi_l - \phi_l\nabla^2\phi_l + \frac{\pi^2}{\eta^2}(\phi_s-\phi_l)\,; \qquad w = \frac{\pi}{\eta}\sqrt{\phi_s\phi_l}\,; \qquad \Delta G_{sl} = -f_s(\vec{c}_s) + f_l(\vec{c}_l) + \vec{\mu}(\vec{c}_s - \vec{c}_l)$$

where $M^a_{sl}(\vec{n})$ is the anisotropic interfacial mobility between liquid and solid as a function of the interface orientation (described by the normal $\vec{n}$) as $\sigma^a_{sl}(\vec{n})$ is the effective anisotropic surface stiffness. K_{sl} is related to the local curvature of the interface. The thermodynamic driving force ΔG_{sl} depends on the respective bulk contributions $f_s(\vec{c}_s)$ and $f_l(\vec{c}_l)$, $\vec{\mu}$ is the generalized chemical potential introduced to conserve local concentration due to the constraint of quasi-equilibrium. This constraint postulates that all the reduced chemical potentials are the same for the coexisting phase i.e $\vec{\mu} = \vec{\mu}_s(\vec{c}_s(\vec{x})) = \vec{\mu}_l(\vec{c}_l(\vec{x}))$. The evolution of the concentration field is given by:

$$\dot{\vec{c}} = \nabla(\phi_s D_s \nabla\vec{c}_s) + \nabla(\phi_l D_l \nabla\vec{c}_l), \tag{4}$$

where D_{s} and D_{l} are respectively the diffusion coefficients in the solid and liquid phase.

4. Results and discussion

We compared the results of the phase-field and the mesoscopic model for several different configurations. The system consisted of a succinonitrile-2 at%acetone alloy solidifying in a fixed gradient of $G_T = 2\cdot10^4\,\mathrm{K/m}$ with a cooling rate of $\dot{T} = -1.16\,\mathrm{K/s}$ ($V_{\mathrm{pull}} = 58\,\mu\mathrm{m/s}$). The growth was initiated with regularly spaced nuclei injected at the bottom of the domain at an initial supersaturation of 0.20. Several different spacings of the initial nuclei λ_0 and several lateral confinements were used. The computational domain is a moving frame, travelling with the dendrite tips, leaving a minimum distance ahead of the most advanced tip. The

frame height was 500 μm and the tip distance was 100 μm. At the vertical sides a zero flux boundary condition was used in the mesoscopic model and a periodic boundary condition in the phase-field model. A fixed concentration C_0 was imposed at the top boundary and a zero derivative at the bottom boundary. The thermophysical properties of the alloys are identical as used in [13]. The tip selection parameter σ^* for the mesoscopic model was determined from the steady-state tip radius obtained by the phase-field model. For that, we used the tip selection criterion $R_{\mathrm{tip}}^2 V_{\mathrm{tip}} = (d_0 D_{\mathrm{l}})/\sigma^*$, where the tip velocity is known and the liquid concentration at the tip used in the capillary length was determined from the supersaturation $\Omega_0 = (C_{\mathrm{l}}^* - C_0)/((1-k_{\mathrm{p}})C_{\mathrm{l}}^*)$ given by the Ivantsov model (Eq. (1) for $\delta \to \infty$): $\Omega_0 = \mathrm{Iv}(Pe_{\mathrm{tip}})$. We obtained $\sigma^*_{\mathrm{SCN-ace}} = 0.0328$. The grid spacing was 0.5 μm in the phase-field simulations and 2.5 μm in the mesoscopic simulations. For a domain width of 250 μm (shown in Figs. 1 and 2) the computation time for the phase-field simulations was 36 h on 12 CPU cores and for the mesoscopic simulations it was 5 h on a single CPU core. The computations were done on different computers, therefore these values do not give a precise comparison but rather an order of magnitude.

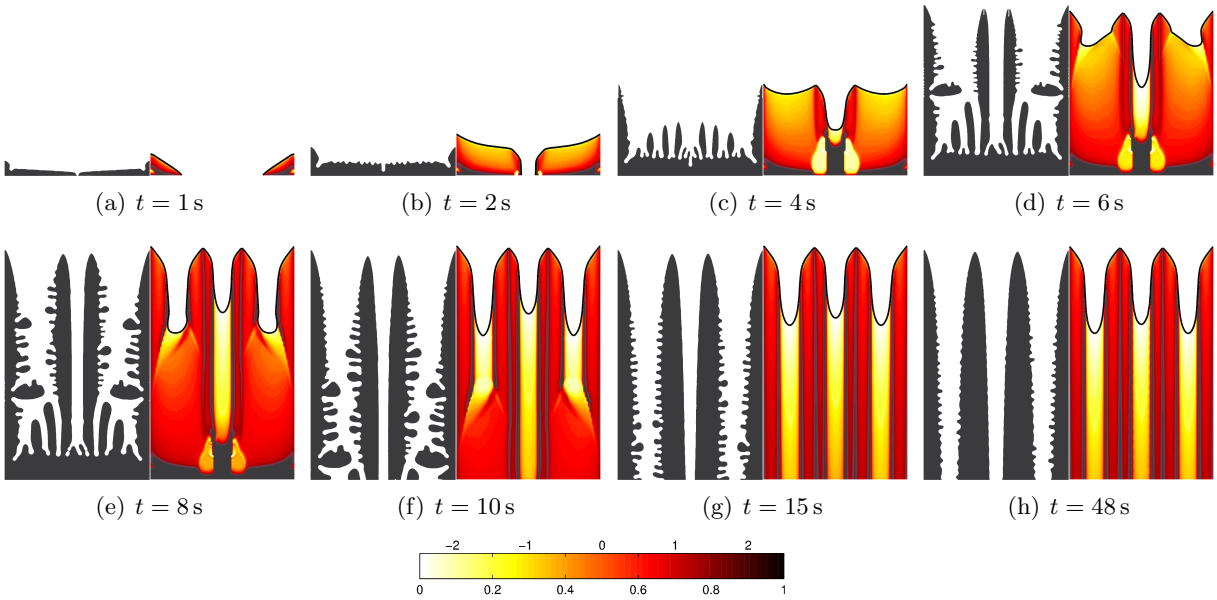

Figure 1. The evolution of the columnar grains from two nuclei placed in the bottom corners. Solid phase calculated by phase field (left) and solid fraction field calculated by the mesoscopic model (right). The domain width is 250 μm.

The columnar growth undergoes an initial transient, during which the tip velocities, the tip undercoolings and the dendrite spacing evolve until a steady state is reached. The transient depends strongly on the spacing of the initial nuclei and on the confinement. To illustrate the transient we show the evolution in the case of SCN-acetone in a confinement of $W = 250\,\mu$m, growing from two nuclei placed in the bottom corners of the domain, i.e. with an initial spacing of $\lambda_0 = 250\,\mu$m, in figures 1 and 2. We can see that after the seeding dendritic branches develop and the horizontal lateral arms first grow very fast along the bottom of the domain, where the supersaturation is the highest. Simultaneously, but initially at a slower rate, vertical primary branches develop in the direction of the temperature gradient. When the tips of the lateral branches meet in the middle of the domain (figure 1(b)), the diffusion fields emanating from the two vertical primary branches have not yet entirely blended (the diffusion time is $\sim (W/2)^2/D_{\mathrm{l}} = 12\,\mathrm{s}$). The supersaturation is thus the highest at mid-distance between the

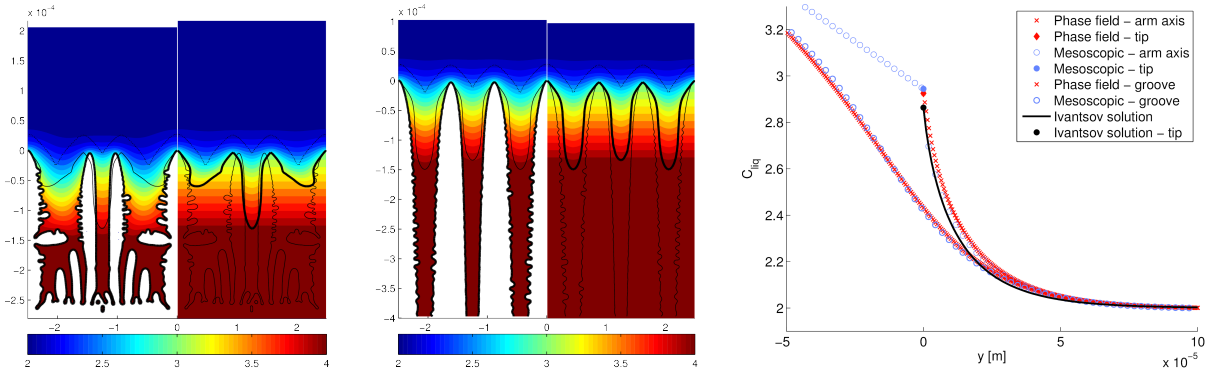

(a) $t = 6\,\mathrm{s}$ (b) $t = 48\,\mathrm{s}$ (c) $t = 48\,\mathrm{s}$

Figure 2. Comparison of concentration fields in the liquid given by the phase-field and the mesoscopic models. (a–b) Field contours (left: phase field, right: mesoscopic). (c) Steady-state concentration profiles along the axis of a primary arm (at $x = 0$) and along a groove between two primary arms (at $x = 125\,\mu\mathrm{m}$), and comparison with the analytical Ivantsov solution.

grains. This drives a fast growth of vertical secondary branches in the middle of the domain (figure 1(c)). In the mesoscopic model this is represented by a vertical expansion of the envelope (at a low solid fraction). Finally, two of the secondary branches prevail and stabilize. In the mesoscopic model this is manifested by the growth of the cusps at the end of the lateral wings of the envelope. In the steady state, attained at approximately $t = 30\,\mathrm{s}$, the tips grow at the rate imposed by the pulling speed of the thermal field ($58\,\mu\mathrm{m/s}$), with a constant tip undercooling and a stable spacing. We can note that the spacing is not uniform but is symmetric.

We performed simulations for several domain widths (lateral confinements) and initial nucleus spacings in order to check the reliability of the spacing selection mechanism reproduced by the mesoscopic model. On the one hand, configurations with an initial spacing larger than the final primary arm spacing ($\lambda_0 > \lambda_1$) were used. In this case the spacing selection proceeds by the development of secondary branches growing vertically from the horizontal lateral arms. The spacing of these branches is small. In a second stage a competition of the secondary branches results first in an increase of the spacing and finally in a stabilisation of a primary spacing. In the mesoscopic model a similar competition of protuberances of the envelope occurs and leads to a stable primary spacing. On the other hand, configurations with ($\lambda_0 < \lambda_1$) were used. In this case, the lateral primary branches are quickly blocked and no significant secondary branching occurs. It is blocked by the diffusion fields emanating from the vertical primary branches, which quickly meet. The spacing selection proceeds by a competition between the vertical primary branches. The phenomenon is reproduced by the mesoscopic model. Simulations initialised with a planar envelope were also performed with the mesoscopic model. After an initial destabilisation of the planar envelope, protuberances with a small spacing develop. They then develop into branches and undergo a competition until a stable primary spacing develops.

The primary spacings obtained in the different configurations are summarized in figure 3. We can see that the final spacing depends not only on the confinement, which can be expected, but also on the initial spacing. The predicted spacings can be compared to classic geometrical models, which give a unique average primary spacing for steady growth as a function of the temperature gradient, the pulling velocity and the solute concentration. They can be resumed by $\overline{\lambda}_1 = a\sqrt{\ell_{\mathrm{sl}} R_{\mathrm{tip}}}$, where the constant a can be alloy-specific [14]. For our configuration different models of this type predict spacings between $32\,\mu\mathrm{m}$ and $150\,\mu\mathrm{m}$; a range across almost an order of magnitude. The predictions of the phase-field and of the mesoscopic model fall

easily within these limits, however their range of variation is much tighter. In contrast to the simple geometrical models, theoretical analyses [15] and experiments [16] showed that a selection mechanism that would uniquely determine the primary spacing does not exist. A given spacing is stable down to a critical minimum velocity.

If we wish to simulate grain interactions, for example interactions of a columnar front with equiaxed grains and the columnar-to-equiaxed transition, an important aspect is a faithful representation of the undercooling field ahead of the columnar front. In figure 2(a–b) we show the solute concentration fields in the liquid around and ahead of the columnar dendrites during the transient and in the steady state. In the left part of each image the concentration field from phase-field and in the right part from the mesoscopic model is shown. The differences in the liquid are relatively small. A more detailed representation is given by a plot of the concentration profiles in the liquid ahead of a primary arm and in the groove along two arms for the steady state in figure 2(c). We can see that the differences are barely perceptible along both profiles. A theoretical Ivantsov solution for an isolated tip is shown for comparison. It shows that the solutal undercooling of the tips of the columnar front is slightly higher than that of an isolated tip. This indicates a slight solutal interaction between the tips. This interaction is captured with good accuracy by both models.

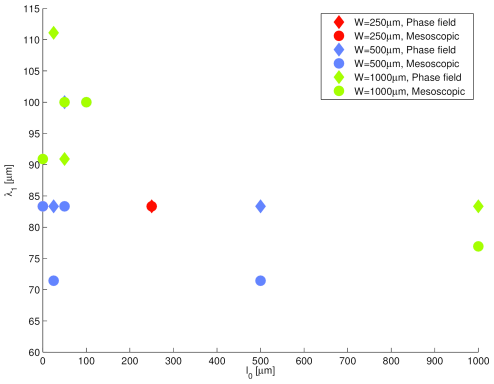

Figure 3. Dependence of the final dendrite spacing on the spacing of the initial nuclei λ_0 and on the width of the confinement W. Mesoscopic simulations with an initially plane front are characterized by an initial spacing $\lambda_0 = 0$.

5. Conclusions and perspectives

We demonstrated the applicability of the mesoscopic envelope model to columnar growth in directional solidification. By comparisons to phase-field computations, used as a reference, we showed that the mesoscopic model: (i) provides a good approximation of the dynamics of the columnar front; (ii) captures the solute diffusion at the scale of the primary spacing and gives an accurate prediction of the solutal undercooling ahead of the columnar tips; (iii) correctly reproduces the phenomena leading to a stable primary spacing by branching and by elimination of branches. The computational cost is substantially smaller than for phase-field computations. The principal reason is the fact that the required grid spacing is around one order of magnitude larger than for the phase-field method.

Further analysis is needed to fully understand the mechanisms of the rebranching of the envelope and of growth competition in the framework of the mesoscopic model. Obvious extensions of this work are 3D computations of columnar growth and the inclusion of fluid flow. Both can be achieved with reasonable computational load. The mesoscopic model can provide a bridge between macroscopic process-scale models and microstructure models, especially in situations involving a strong coupling between the microstructure evolution and the macroscale melt flow.

Acknowledgments

We gratefully acknowledge the support to this research by the German Federal Ministry of Research through the German Space Agency DLR under Contract FKZ 50WM1143. This work was supported by the French State through the program "Investment in the future" operated by the National Research Agency (ANR) and referenced by ANR-11 LABX-0008-01 (LabEx DAMAS).

References

[1] Steinbach I, Beckermann C, Kauerauf B, Li Q and Guo J 1999 *Acta Mater.* **47** 971–982
[2] Steinbach I, Diepers H J and Beckermann C 2005 *J. Cryst. Growth* **275** 624–638
[3] Delaleau P, Beckermann C, Mathiesen R H and Arnberg L 2010 *ISIJ Int.* **50** 1886–1894
[4] Souhar Y, De Felice V F, Založnik M, Combeau H and Beckermann C 2015 *IOP Conf. Series: Mater. Sci. Eng.* (in press)
[5] Tourret D and Karma A 2013 *Acta Mater.* **61** 6474–6491
[6] Kharicha A, Stefan-Kharicha M, Wu M and Ludwig A 2012 *IOP Conf. Series: Mater. Sci. Eng.* **33** 012115
[7] Steinbach I 2008 *Acta Mater.* **56** 4965–4971
[8] Cantor B and Vogel A 1977 *J. Cryst. Growth* **41** 109–123
[9] Sun Y and Beckermann C 2007 *J. Comput. Phys.* **220** 626–653
[10] Beckermann C and Viskanta R 1993 *Appl. Mech. Rev.* **46** 1–27
[11] Steinbach I, Pezzolla F, Nestler B, Seeßelberg M, Prieler R, Schmitz G and Rezende J 1996 *Physica* D **94** 135–147
[12] Eiken J, Böttger B and Steinbach I 2006 *Phys. Rev.* E **73** 066122
[13] Melendez A J and Beckermann C 2012 *J. Cryst. Growth* **340** 175–189
[14] Steinbach S 2005 *Einfluss von Strömungen auf die Entwicklung des Mikrogefüges bei der gerichteten Erstarrung von Al-Si und Al-Si-Mg Legierungen* Ph.D. thesis RWTH Aachen
[15] Warren J A and Langer J S 1993 *Phys. Rev.* E **47** 2702–2713
[16] Losert W, Shi B Q, Cummins H Z and Warren J A 1996 *Phys. Rev. Lett.* **77** 889–891